Materials Science and Engineering A xxx (2009) xxx–xxx

Contents lists available at ScienceDirect

Materials Science and Engineering A

journal homepage: www.elsevier.com/locate/msea

Characteristics of martensite as a function of the M_S temperature in low-carbon armour steel plates

Kasonde Maweja[a,b,*], Waldo Stumpf[b], Nic van der Berg[c]

[a] The Council for Scientific and Industrial Research, CSIR, Materials Science and Manufacturing, PO Box 395, Pretoria 0001, South Africa
[b] Department of Materials Science and Metallurgical Engineering, University of Pretoria, Pretoria 0002, South Africa
[c] Department of Physics, University of Pretoria, Pretoria 0002, South Africa

ARTICLE INFO

Article history:
Received 17 December 2008
Received in revised form 25 April 2009
Accepted 29 April 2009
Available online xxx

Keywords:
Martensite
Morphology
Microstructure
Ballistic performance

ABSTRACT

The microstructure, morphology, crystal structure and surface relief of martensite in a number of experimental armour steel plates with different M_s temperatures were analysed. Atomic force microscopy, thin foil transmission electron microscopy and scanning electron microscopy allowed the identification of three groups of low-carbon martensitic armour steels. The investigation showed that the size of individual martensite products (plates or packets, laths or blocks) increases as the M_s temperature increases. Comparison of ballistic performances suggests that the morphology (plate or lath) and size of the individual martensite products dictate the effective "grain size" in resisting fracture or perforation due to ballistic impact.

1. Introduction

In prior work current design approaches, which are largely based on the mechanical properties of the armour steel such as the ultimate tensile strength, the sub-zero Charpy-V impact energy and the hardness [1–4], were not successful in predicting the ballistic performance of a number of currently produced martensitic armour plate steels with a thickness of 6 mm. It was found that high hardness or high mechanical properties were not reliable factors in predicting their ballistic performance [3–6]. A morphological/microstructural approach is hence rendered necessary to enable the prediction of the ballistic performance and to reduce the design duration and cost of developing new armour steels. Recent studies on the ballistic performances of armour steels, the alloy Ti–6Al–4V, diverse composites, ceramics and carbon-nanotube reinforced polyvinyl-ester have demonstrated how necessary it becomes to integrate the relationship between microstructures and material behaviour upon ballistic performance in modelling of materials for this purpose [7–17]. Even the knowledge of the electronic structure of the material would become important in predicting the material's behaviour upon ballistic impact according to a recent suggestion [13].

The microstructural and morphological characteristics of five low-carbon martensitic armour steels were analysed in the present work to understand the differences in their performance upon ballistic testing. The compositions of the experimental armour steels were selected to cover a wide range of M_s temperatures corresponding largely to current commercial armour steels in plate form. The martensite start temperature is a function of the chemical composition of the steel and the austenitisation temperature. It may, therefore, be used as an indirect variable that categorises the steels by combining the effects of the chemical composition and the austenitisation conditions into one variable.

Thermodynamic and experimental data [18,19] have predicted a change in the morphology of the martensite at M_s temperatures between 232 and 284 °C for different Fe–C alloys. The simultaneous formation of lath and plate martensite within this M_s temperature range would minimise the transformation strain energy in comparison to either the formation of only lath martensite or plate martensite respectively. Xiaoping et al. [20] have determined the crystallographic characteristics by using atomic force microscopy (AFM), of $\{2, 5, 9\}_\gamma$ and of $\{2, 2, 5\}_\gamma$ martensite in an Fe–23%Ni–0.55%C and an Fe–8%Cr–1%C alloy respectively. They observed that the relief angles of $\{2, 5, 9\}_\gamma$ and $\{2, 2, 5\}_\gamma$ martensite range from 4° to 5.8° and from 1° to 9° respectively.

Taking the above into account, two experimental armour steels falling within this transition temperature range were, therefore, chosen while another two had their M_s temperatures below this range and the fifth one above.

* Corresponding author at: PO Box 100026, Moreleta Plaza, Pretoria 0167, South Africa. Tel.: +27 83 365 0952.
E-mail address: mawejak@yahoo.fr (K. Maweja).

0921-5093/$ – see front matter © 2009 Elsevier B.V. All rights reserved.
doi:10.1016/j.msea.2009.04.061

Table 1
Chemical composition in wt.% of the armour steels in plate form. Balance Fe.

Steel	C	Mn	P	S	Si	Cu	Ni	Cr	Mo	V	Nb	Ti	N
G1A	0.39	1.22	0.008	0.003	0.21	0.102	2.99	1.49	0.5	0.006	0.002	0.003	0.0049
G1B	0.37	1.15	0.015	0.011	1.06	0.14	3.8	0.52	0.43	0.008	0.008	0.007	0.0036
G2A	0.39	0.65	0.017	0.009	0.8	0.23	2.8	0.22	0.24	0.003	0.006	0.01	0.0051
G2B	0.37	0.40	0.016	0.011	0.43	0.33	2.3	0.24	0.3	0.006	0.006	0.009	
G3	0.34	0.39	0.019	0.012	0.40	0.32	2.43	0.27	0.37	0.009	0.009	0.008	

Table 2
Measured M_s temperatures and volume fractions of retained austenite (RA) after quenching.

	Steel				
	G1A	G1B	G2A	G2B	G3
M_s (°C)	196	210	255	271	309
Volume fraction of RA (%)	5	4	0.6	0.5	0.5
a_γ (nm)	0.3645	0.3656	0.3656	0.3683	0.3683
a_m (nm)	0.2867	0.2862	0.2864	0.2865	0.2866

Table 3
Measured M_s temperatures of the armour steels G1A to G3 and the corresponding transformation characteristics deduced from [18,19].

Steel	M_s (°C)	Habit plane
G1A	196	{2, 5, 9}-twinning in ferrite
G1B	210	{2, 5, 9}-twinning in ferrite
G2A	255	{2, 2, 5}-slip in austenite and twinning in ferrite (butterfly martensite)
G2B	271	{2, 2, 5}
G3	309	{1, 1, 1}-slip in austenite and ferrite (lath martensite)

2. Materials and experiments

Experimental 4.5 kg ingots were vacuum induction melted and cast into ingots which were then austenitised for 1 h at 1100 °C before hot rolling down to a nominal 6 mm thickness in four passes, ending between 900 and 950 °C, and the hot rolled plates were then water quenched. The average chemical compositions of the five armour steels determined by three different techniques, i.e. atomic absorption spectroscopy, wet analysis and Leco analysis are shown in Table 1.

The two steels with their M_s temperature within the above transition range are identified within Group 2 as steels G2A and G2B while the two with M_s temperatures below this range are identified within Group 1 as steels G1A and G1B while the fifth steel with a M_s above this range is identified within Group 3 as the steel G3.

Microstructural and morphological analyses were conducted by means of three different techniques to gain an insight into the differences in martensite morphology between these five experimental armour steels. Thin foils for TEM analysis were prepared from discs wire-cut from these quenched plates. These discs were electropolished at 0 °C in a solution of 6 vol.% perchloric acid and 0.5 vol.% chromium oxide in glacial acetic acid. The thin foils were examined in a PHILIPS CM 200 TEM at accelerating voltage of 160 kV. The SEM samples were polished mechanically and etched for 7 s

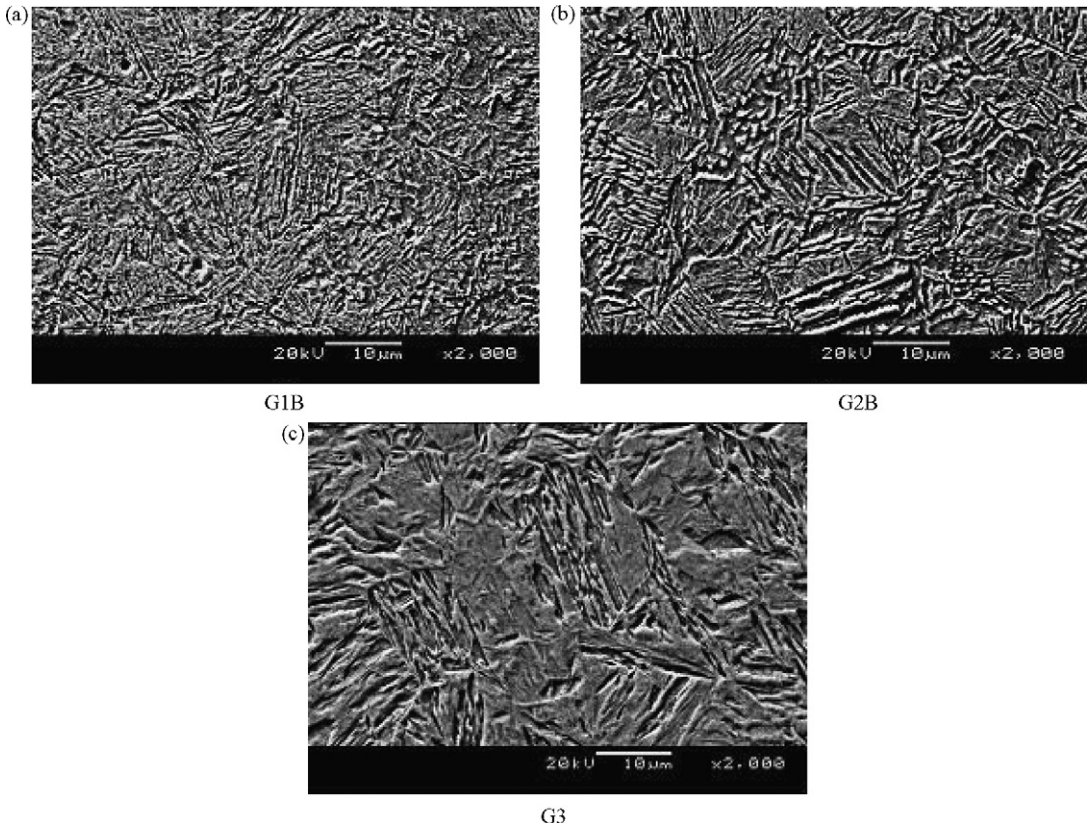

Fig. 1. Backscattered scanning electron microscopy of (a) steel G1B with M_s = 210 °C, (b) steel G2B with M_s = 271 °C and (c) steel G3 with M_s = 309 °C.

Please cite this article in press as: K. Maweja, et al., Mater. Sci. Eng. A (2009), doi:10.1016/j.msea.2009.04.061

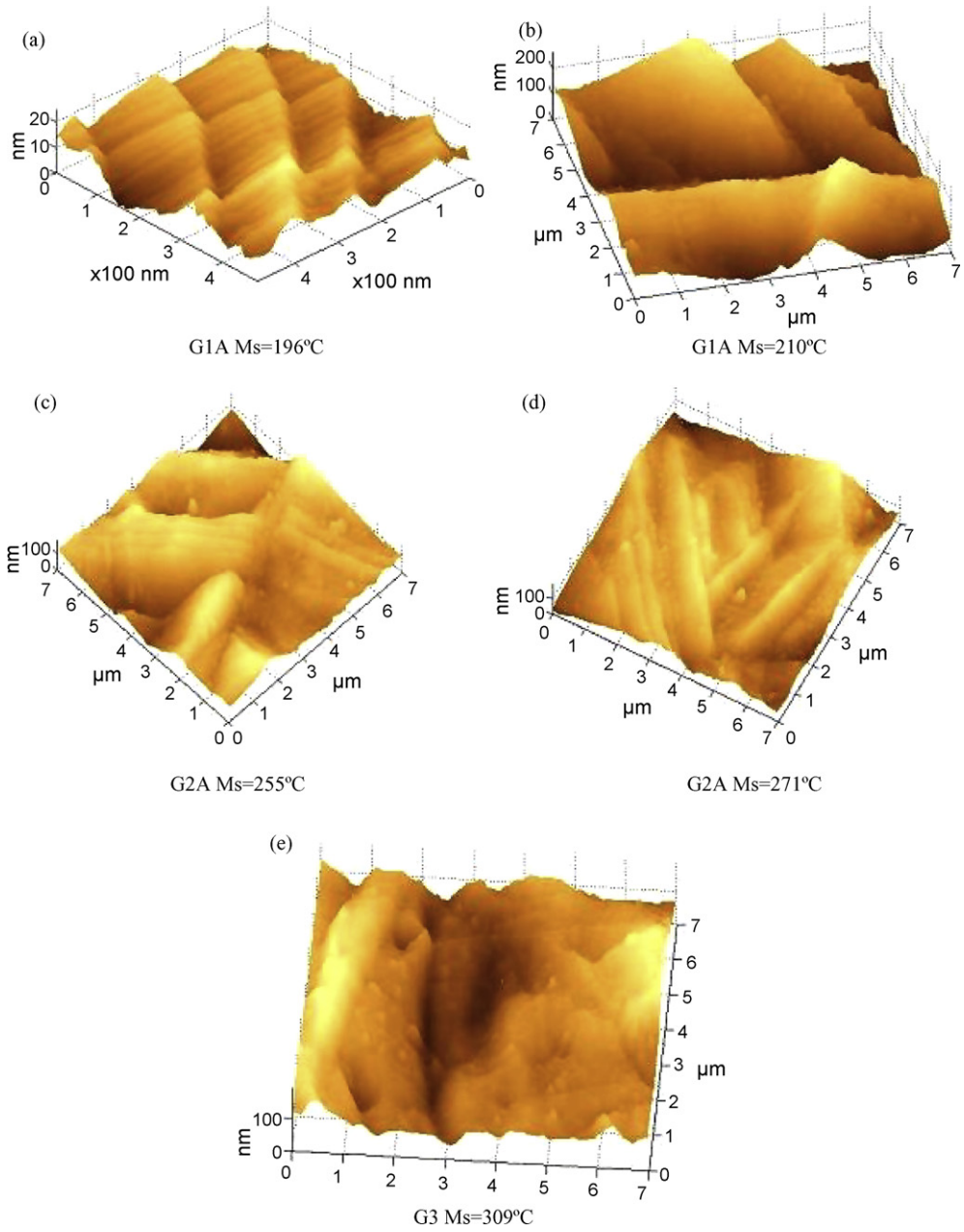

Fig. 2. AFM topography of (a) steel G1A with M_s = 196 °C, (b) steel G1B with M_s = 210 °C, (c) steel G2A with M_s = 255 °C, (d) steel G2B with M_s = 271 °C, and (e) steel G3 with M_s = 309 °C.

with a 2% Nital solution and analysed in a Philips scanning electron microscope. The samples for atomic force microscopy were prepared from the 15 mm × 10 mm × 2 mm specimens cut from the hot rolled and quenched plates. These specimens were mechanically grinded, then polished with a 1 μm diamond paste and finally electropolished in a solution of 5 vol.% perchloric acid and 95 vol.% glacial acetic acid at 0 °C to minimise the initial surface roughness and to remove any mechanically induced martensite from the retained austenite. These polished samples were then austenitised for 10 min at 900 °C, in a high vacuum in a THETA 734 Single Silica Push Rod LVDT dilatometer and quenched to room temperature in a fast but regulated flow of helium gas. The M_S temperatures of the steels were determined via the fast cooling path of the dilatometer graphs. The surface relief features on the previously polished faces were measured in air at room temperature on a nanometre scale using the atomic force microscope Topometrix TMX 2000 "Discoverer". The Fast Fourier Transform implemented by the discrete Fourier transform algorithm was used to analyse the periodicity of the surface relief by using MATLAB 7.0 software. X-ray diffraction in an X'Pert PRO PANalytical equipment was used to determine the phases present (particularly the % retained austenite) in the steels and their lattice parameters. The results of the above analyses were finally correlated to the ballistic performances reported in [6,21].

3. Results and discussion

3.1. Martensite start temperatures, crystal and microstructures of the five experimental armour steels

The M_S temperatures and the volume fractions of retained austenite (RA) after water quenching of the armour steels are shown in Table 2. The martensite had a BCC crystal structure in all of the five armour steels at room temperature and no measurable tetragonal-

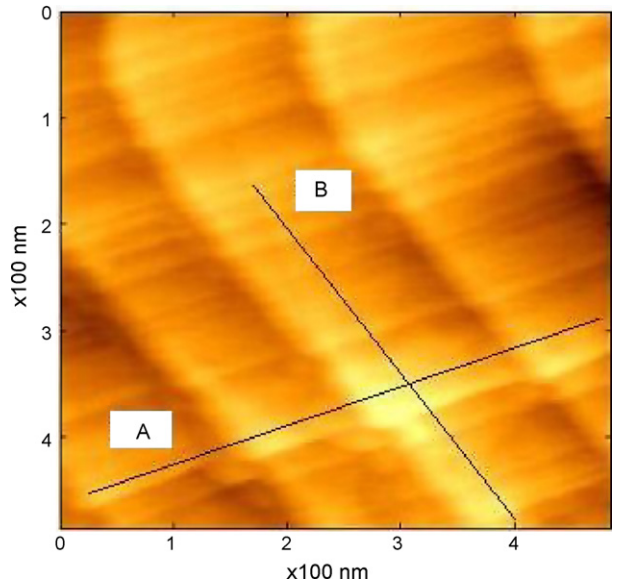

Fig. 3. AFM topography of steel G1A with M_s = 196 °C, showing the larger set of twins formed normal to the direction (A) and another family of sub-twins formed normal to the direction (B).

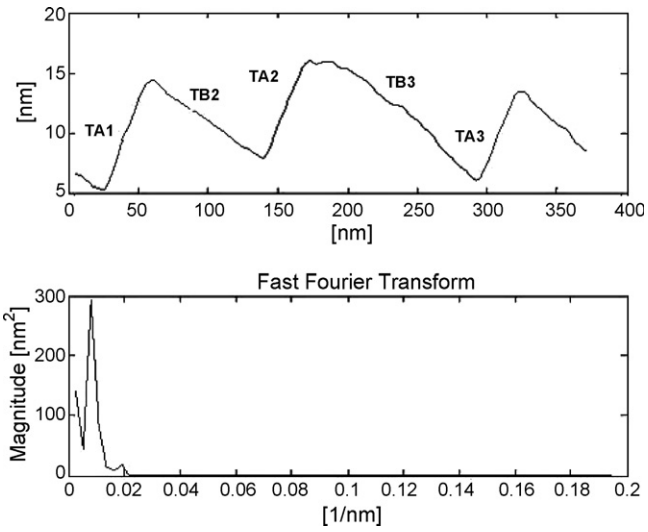

Fig. 4. Surface relief profile of steel G1A along the normal direction to A and the corresponding Fast Fourier Transform.

ity was observed in the specimens that were immediately analysed after water quenching. Comparison to the results reported earlier in [18,19] and shown in Table 3, suggests that plate and lath martensite would coexist in steels G2A and G2B of which the M_s temperatures were measured as 255 and 271 °C respectively. The typical microstructures corresponding to the three groups of armour steels, i.e. G1B, G2B and G3 are compared in Fig. 1. The microstructure of Fig. 1(a) suggests that the martensitic structure of steel G1B with M_s of 210 °C consisted largely of thin plates while that of steel G2B contained both plate and lath areas. The widths of the plates became larger as the M_s increased to 271 °C as shown in Fig. 1(b). However, predominantly lath morphology was observed in the higher M_s steel G3 as shown in Fig. 1(c). The carbon content of the five experimental armour steels varied only from 0.34 to 0.39 wt.% with little variation in actual tetragonality or the Bain strains of the martensite between the five steels expected. However, the difference in morphology of the martensite was noticeable. This is attributed to a stronger dependence of the martensite morphology on the M_s temperature (which is a function of the entire chemistry) and which varied from 196 to 309 °C, rather than on the carbon content of the steel only.

3.2. Atomic force microscopy of the surface relief and transmission electron microscopy of the five experimental armour steels

The surface relief accompanying the martensite formation in the five steels is shown in Fig. 2, arranged by order of increasing M_s. The standard roughness Rtm of the electropolished surfaces before martensitic transformation varied between 3.8 and 5.0 nm. Twinned martensite with fine substructures that formed along a direction quasi-parallel to the habit plane of the twin structure, were observed in large areas of the steel G1A, which had the lowest M_s temperature of 196 °C. Characteristic surfaces of the steels G1A and G1B are regular N-shaped with sharp edges. No twin substructures were observed in the four amour steels with M_s temperatures that were above 200 °C. The AFM images show different surface topographies in different areas of the steels within the transition group G2 as illustrated in Fig. 2(c) and (d), suggesting the possible simultaneous formation of the martensite by slip and twinning mechanisms or by a more complex mechanism yet to be defined. Some areas are N-shaped but with round edges while a twin type topography in lath martensite could be observed in an isolated area of the steel G2B with a M_s temperature of 271 °C. The growth of these twinned plates was stopped on boundaries with the non-deformed retained austenite. A typical surface relief of lath martensite of steel G3 with the highest M_s temperature of 309 °C is shown in Fig. 2(f).

Table 4
Measured geometric characteristics of the twins along two lines normal to the direction A (see Fig. 3) in steel G1A.

Line 1	TA_1	TB_2	TA_2	TB_3	TA_3
d*x* (nm)	35.7151	79.615	33.4829	24.5542	95.9844
Height (nm)	9.0587	−6.4442	8.0391	−8.7580	7.3517
Relief angle (°)	14.23	−4.62	13.50	−4.84	13.55
Width (nm)	36.846	79.875	34.434	55.848	26.425
Slope (nm/°)	2.58	−17.25	2.54	−11.6	1.94
Twinning ratio TB/(TB + TA)		0.69		0.68	

Line 2	TA_1	TB_1	TA_2	TB_2	TA_3	TB_3
d*x* (nm)	35.6789	79.7081	26.5694	92.6132	31.1241	55.4161
Height (nm)	9.1765	−6.5073	6.644	−9.066	7.3783	−5.6099
Relief angle (°)	14.43099	−4.66959	14.04671	−5.59376	13.34315	−5.78342
Width (nm)	36.84009	79.97328	27.38751	93.05588	31.9867	55.69933
Slope (nm/°)	2.55	−17.12	2.00	−16.63	2.39	−9.63
Twinning ratio TB/(TB + TA)	0.74		0.74		0.63	

Please cite this article in press as: K. Maweja, et al., Mater. Sci. Eng. A (2009), doi:10.1016/j.msea.2009.04.061

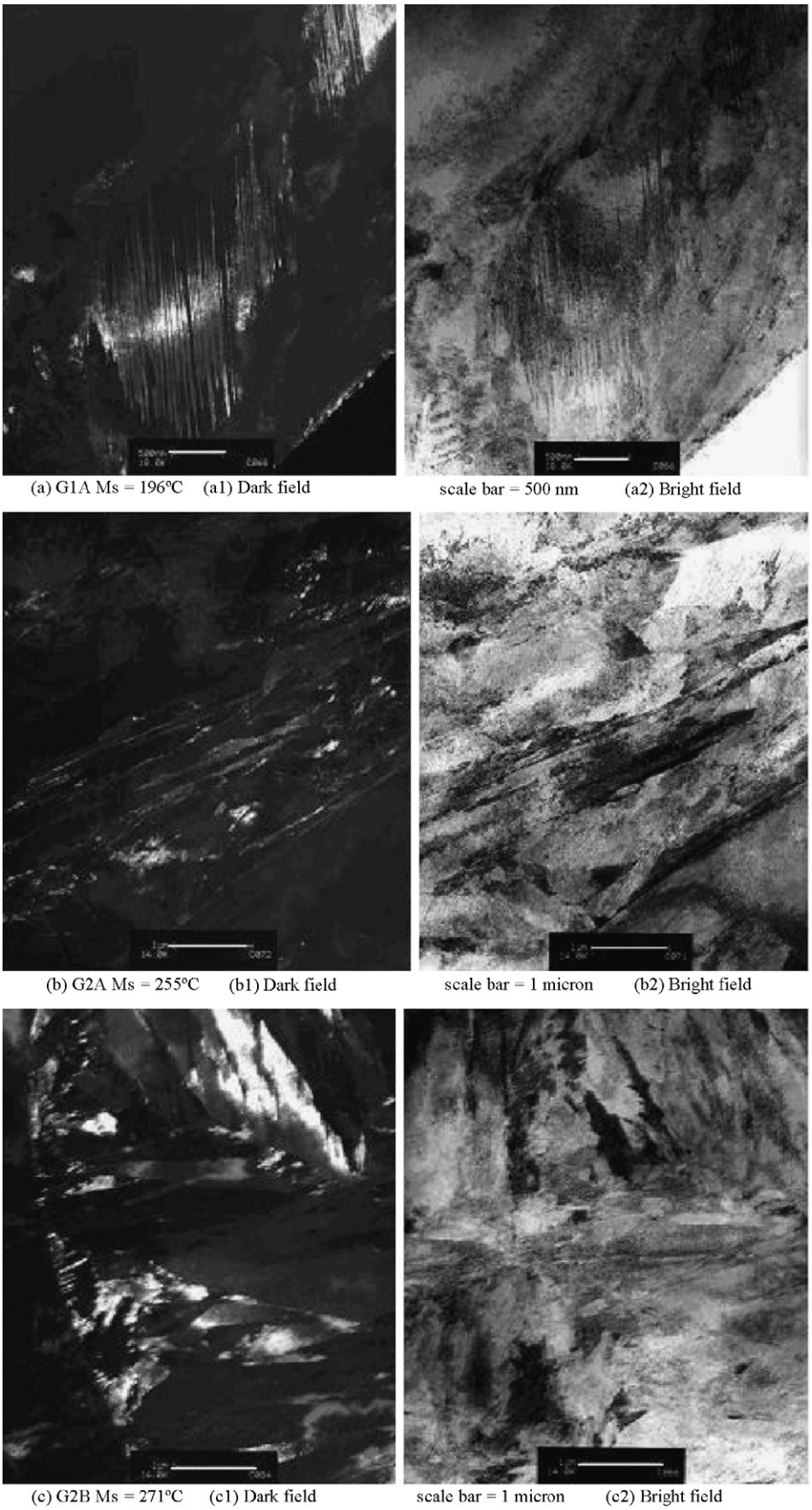

Fig. 5. Thin foil transmission electron micrographs showing the morphology of the martensite and retained austenite (RA) in steels G1A through to G3 after water quenching from 900 °C. Magnification ×5000. Foils for dark field micrographs were oriented to show the "white" retained austenite.

Please cite this article in press as: K. Maweja, et al., Mater. Sci. Eng. A (2009), doi:10.1016/j.msea.2009.04.061

(d) G3 Ms = 309°C scale bar = 500 nm

Fig. 5. (*Continued.*)

The mechanism of formation of the martensite changed to one of single twinning when the M_s reached about 210 °C as illustrated in Fig. 2(b). For the M_s temperatures of 255 and 271 °C in Fig. 2(c) and (d) respectively, twinned martensite was formed together with lath martensite. The rounded edges of the surface relief may be due to a significant rotation of the habit plane during the martensitic transformation to accommodate the transformation strain and to a change in the formation mechanism of the martensite (while keeping in mind, however, that only the surface behaviour of new martensite formation is determined by AFM and not necessarily the behaviour within the specimen where more degrees of restraint are present from the bulk). This transition topography also lies well within the M_s transition range reported in the literature by Mou and Aaronson [19]. The topography of the surface of steel G3 in Fig. 2(e) with M_s = 309 °C, can be attributed to the plastic strain resulting from the slip of dislocations and a large rotation of the habit plane. But significant diffusion of carbon atoms near the surface during quenching (auto-tempering) may also be the cause of such rounded edges as suggested by Krauss [22].

It was pointed out for the steel G1A in Fig. 2(a) (M_s of 196 °C), that two internal twin families were formed along two different directions. The twinning ratios of these two families were measured and their spatial frequencies were determined using the Fast Fourier Transform. Normal lines were considered relative to each direction A or B as shown in Fig. 3. The typical surface relief profile along direction A and the corresponding Fast Fourier Transform is presented in Fig. 4, for the direction normal to A. The geometrical characteristics of the twins are given in Table 4 where (dx) is the horizontal distance between a minimum and the following maximum or vice versa and (dy) is the height difference between the two points. The twinning ratio $TB_i/(TB_i + TA_i)$ along the direction normal to A in steel G1A is 0.69 ± 0.06. Twins TB_i are regular shapes whose relief angle is about $5.2 \pm 0.6°$. Twins TA_i are also regular shapes but their relief angle is about $13.5 \pm 2.0°$. The frequency spectrum contains a narrow bandwidth peak at about 0.008 nm^{-1}. This indicates that the twinned plates ($TB_i + TA_i$) are not exactly the same width but are rather continuously distributed around a mean width of 125 nm.

The twinning ratio along the direction normal to B in steel G1A is 0.56 ± 0.03. The surface relief was again N-shaped with twins TB_i whose relief angle was about $5.0 \pm 1.0°$ and twins TA_i whose relief angle was about $6.0 \pm 2.0°$. The width of the twins in the direction normal to B ranges from 60 to 90 nm, which is smaller than the 125 nm measured normal to the direction A. The twinning ratio is smaller along the direction normal to B than along the direction normal to A. The relief angles measured here for steel G1A, which ranged from 4° to 6°, correspond well to those measured by Xiaoping et al. [20], for the $\{2, 5, 9\}_\gamma$ martensite. However, the widths of the plates measured for steel G1A ranging from 90 to 125 nm, were at least two times smaller than those reported by Xiaoping et al. It appears from this comparison that the relief angle of the $\{2, 5, 9\}_\gamma$ martensite may be less sensitive to the chemical composition than the width of the plates. Moreover, it appears from comparison between these measurements and the results reported by Xiaoping et al., that the austenitisation temperature may have an effect on the widths of the martensite plates but not on the relief angles.

Thin foil transmission electron microscopy of the five steels also revealed that different martensite morphologies were indeed formed upon water quenching of these low-carbon armour steels. Fig. 5 shows the observed typical morphologies as the M_s temperatures of the hot rolled and quenched steels increased from 196 to 309 °C. Steels G1A and G1B with M_s = 196 °C and 210 °C respectively, contained twinned martensite with some nodular retained austenite. Steel G2A with M_s = 255 °C contained butterfly martensite while lath martensite became the dominant morphology in steel G2B with M_s = 271 °C with films of retained austenite present in some areas of the latter steel. Transmission electron microscopy of steel G3 with M_s = 309 °C showed a predominant auto-tempered lath martensite morphology.

Comparison of the martensite features given in Fig. 1 (SEM), Fig. 2 (AFM) and Fig. 5 (TEM) suggests that low-carbon martensitic armour steels could well be grouped into three categories of martensite morphology, i.e. G1, G2 and G3 with respect to the martensite transformation temperatures. Furthermore, it also appears from the investigation that the size of the individual martensite products (plates or packets, laths or blocks) increases as the M_s temperature increases.

3.3. Ballistic performance

Mechanical properties and ballistic performances of the 6 mm thick plates from these five and another eight experimental and

Please cite this article in press as: K. Maweja, et al., Mater. Sci. Eng. A (2009), doi:10.1016/j.msea.2009.04.061

Table 5
Ballistic performance of the plates tested by 5.56 mm standard R4 fired from 30 m under 0° obliquity [6].

Plate designation	UTS (MPa)	Elongation%	VHN (30 kg)	Projectile velocity (m/s)	Ballistic performance
G1A	1650	4	578	945 ± 10	Passed fully
G1B	1700	6	565	945 ± 10	Passed fully
G2A	2200	8	610	945 ± 10	3/5 Failed*
G2B	2000	12	520	945 ± 10	Failed
G3	1700	14	490	945 ± 10	Failed

* Three out five rounds failed by penetration of the 6 mm plate.

three commercial armour steels were reported in [6,21]. Table 5 extracted from the ballistic report [6] is quoted here.

It appears from the ballistic report that the plate martensite microstructures formed at lower M_s temperatures offered the best performance against ballistic impact. Close inspection of the impacted regions also revealed that the finer the individual martensite features (twinned plates) are, the higher the resistance against ballistic perforation and against crack propagation along the grain boundaries will be. The high ballistic performance of the low M_s steels was in part attributed to the capacity of energy absorption by strain induced transformation of the retained austenite [5,6,21]. A more coarse lath martensite microstructure of steel G3 (high M_s) is not conducive for a high resistance to ballistic perforation of the 6 mm thick armour steel plates. The transition microstructures of Group 2 steels (220 °C < M_s < 270 °C) do not provide full ballistic protection at this thickness despite them having the best combination of strength, elongation and hardness of all as shown in Table 5. Full ballistic protection of low-carbon alloyed armour steel plates of 6 mm thickness appears to be only assured in Group 1 steels with M_s temperatures below the transition range, i.e. below about 220 °C where some retained austenite is present and the martensite morphology is one of $\{2, 5, 9\}_\gamma$ twinning.

4. Conclusions

1. Three different predominant morphologies of the martensite were identified in the microstructures of the low-carbon and alloyed armour steels as the M_s temperature increased from 196 to 309 °C. The martensite morphology and the size of the individual plates and laths in these steels also depend on the M_s temperature, hence on the complete chemistry of the alloys rather than on the carbon content alone.
2. Predominantly $\{2, 5, 9\}_\gamma$ twinned plate martensite had a superior ballistic performance than the mixed martensitic microstructure in steels with M_s temperatures between 210 and 255 °C while even lower ballistic performances were recorded for the lath martensite with a M_s temperature higher than 255 °C. Lath martensite and large sized martensitic microstructural features are likely to be less resistant to ballistic perforation and spallation, possibly due to their influence on the micro-geometry and the character of the grain boundaries. The size of the martensite plates or laths might also, therefore, have an influence on the performance in resisting fracture or perforation due to ballistic impact.

Acknowledgements

The authors would like to thank ArcelorMittal (South Africa) and the Technology and Human Resources for Industry Program, THRIP of the South African National Research Foundation for their logistic and financial support. The kind assistance of Dr S Verryn and Ms Alison Tuling in the XRD and TEM work and Mr C Coetzee in the SEM work is also kindly acknowledged. Finally, the permission of both ArcelorMittal (South Africa) and the University of Pretoria to publish this work is appreciated.

References

[1] Mittal Steel South Africa, Technical notes, 2003.
[2] S.P. Wolsky, A.W. Czanderna, Methods and Phenomena 5 Ballistic Materials and Penetration Mechanics, Elsevier Scientific Publishing Company, 1982.
[3] B. Srivathsa, N. Ramakrishnan, Journal of Materials Processing Technology 96 (1999) 81–91.
[4] B. Srivathsa, N. Ramakrishnan, Computer Simulation Modelling in Engineering 3 (1998) 33–40.
[5] K. Maweja, W. Stumpf, Materials Science and Engineering: A 432 (2006) 158–169.
[6] K. Maweja, W. Stumpf, Materials Science and Engineering: A 485 (2008) 140–153.
[7] C.Y. Sun, G. Fang, L.P. Lei, P. Zeng, Materials Science and Engineering: A 499 (2009) 18–22.
[8] P.K. Jena, K. Siva Kumar, V. Rama Krishna, A.K. Singh, T. Balakrishna Bhat, Engineering Failure Analysis 15 (2008) 1088–1096.
[9] A. Kar, M. Ghosh, Ashok Kumar Ray, Ajoy Kumar Ray, Materials Science and Engineering: A 498 (2008) 283–288.
[10] T. Demir, M. Übeyli, R. Orhan Yıldırım, Materials & Design 29 (2008) 2009–2016.
[11] O. Çoban, M. Özgür Bora, T. Sinmazçelik, I. Cürgül, V. Günay, Materials & Design 30 (2009) 628–663.
[12] X. Liu, C. Tan, J. Zhang, Y. Hu, H. Ma, F. Wang, H. Cai, Materials Science and Engineering: A 501 (2009) 30–36.
[13] B.S. Yılbas, İ.T. Dolapçı, M. Pakdemirli, International Journal of Thermal Sciences 48 (2009) 383–390.
[14] B. Bhav Singh, K. Sivakumar, T. Balakrishna Bhat, International Journal of Impact Engineering 36 (2009) 611–620.
[15] L. Zhen, G.A. Li, D.L. Zou, W.Z. Shao, Materials Science and Engineering: A 489 (2008) 213–219.
[16] N.K. Bourne, International Journal of Impact Engineering 35 (2008) 674–683.
[17] M. Grujicic, W.C. Bell, L.L. Thompson, K.L. Koudela, B.A. Cheeseman, Materials Science and Engineering: A 479 (2008) 10–22.
[18] R.G. Davies, C.L. Magee, Metallurgical Transactions 2 (1971) 1939.
[19] Y. Mou, H.I. Aaronson, Acta Metallurgica 37 (3) (1989) 737–765.
[20] L. Xiaoping, G. Nanju, Z. Yong, M. Zhaowei, M. Xiaoli, Progress in Natural Science (2002).
[21] K. Maweja, W. Stumpf, Materials Science and Engineering: A 480 (2008) 160–166.
[22] G. Krauss, Materials Science and Engineering: A 273–275 (1999) 40–57.